

# Crystal structure and crystal-chemistry of vanadio-pargasite: a new amphibole from southern Lake Baikal, Siberia, Russia

GEORGIA CAMETTI<sup>1,\*</sup>, THOMAS ARMBRUSTER<sup>1</sup>, LEONID Z. REZNITSKY<sup>2</sup>, EVGENY V. SKLYAROV<sup>2,3</sup> and GIANCARLO DELLA VENTURA<sup>4,5</sup>

<sup>1</sup> Mineralogical Crystallography, Institute of Geological Sciences, University of Bern Baltzerstr. 1+3, Bern 3012, Switzerland

\*Corresponding author, e-mail: [georgia.cametti@krist.unibe.ch](mailto:georgia.cametti@krist.unibe.ch)

<sup>2</sup> Institute of the Earth's Crust, Siberian Branch of the Russian Academy of Science, Irkutsk 664033, Russia

<sup>3</sup> Far East Federal University, 8 Sukhanova Str., Vladivostok 690091, Russia

<sup>4</sup> Dipartimento di Scienze, University of Roma Tre, Rome, Italy

<sup>5</sup> LNF-INFN, Frascati (Rome), Italy

**Abstract:** The crystal structure of a new member of the calcium amphibole subgroup, vanadio-pargasite ideally  $\text{NaCa}_2(\text{Mg}_4\text{V}^{3+})\text{Si}_6\text{Al}_2\text{O}_{22}(\text{OH})_2$  with empirical formula  $(\text{K}_{0.07}\text{Na}_{0.90})(\text{Na}_{0.05}\text{Ca}_{1.91}\text{Mg}_{0.04})\Sigma_{2.00}(\text{Mg}_{4.02}\text{Cr}_{0.05}\text{V}_{0.68}\text{Al}_{0.23}\text{Ti}_{0.02})\Sigma_{5.00}(\text{Si}_{6.09}\text{Al}_{1.91})\Sigma_{8.00}\text{O}_{22}(\text{OH}_{1.67}\text{F}_{0.33})\Sigma_{2.00}$ , was studied by single-crystal X-ray diffraction and refined to  $R1$  of 0.0181. It is monoclinic, space group  $C2/m$ , unit-cell parameters  $a = 9.8956(1)$ ,  $b = 17.9970(2)$ ,  $c = 5.2970(1)$  Å,  $\beta = 105.391(1)^\circ$ , and  $V = 909.52$  Å<sup>3</sup>. The mineral is isostructural with the amphiboles pargasite, magnesio-hastingsite, chromio-pargasite and  $\text{Mn}^{3+}$ -rich pargasite. Site populations were derived from the structure refinement and electron-microbe analysis, and validated on the basis of OH-stretching FTIR spectroscopy. Accordingly, V is ordered at  $M(2)$  together with minor <sup>[6]</sup>Al, while a low amount of <sup>[6]</sup>Al is present at  $M(3)$ .

**Keywords:** vanadio-pargasite; new mineral; crystal structure; amphibole; infrared; vanadium.

## 1. Introduction

Vanadio-pargasite, ideally  $\text{NaCa}_2(\text{Mg}_4\text{V}^{3+})\text{Si}_6\text{Al}_2\text{O}_{22}(\text{OH})_2$ , was recently discovered in the Pereval marble quarry, Irkutsk region, southern Lake Baikal, Siberia, Russia. The new mineral has been approved by the Commission on New Minerals, Nomenclature and Classification (CNMNC) of the International Mineralogical Association (IMA) (No. 2017-019). The host rocks (marble) are Cr–V-bearing calcite-dolomite with siliceous sediments, metamorphosed in granulite facies and partly diaphorised in amphibolite facies. Vanadio-pargasite is thought to be formed during the prograde (granulite-facies) stage. A detailed description of its occurrence, chemistry and mineralogical features was presented by Reznitsky *et al.* (2017).

Among monoclinic  $C2/m$  amphiboles with Ca dominant as B cation (calcium amphiboles), the root names pargasite and hastingsite refer to  $\text{NaCa}_2(\text{Mg}_4\text{Al})(\text{Si}_6\text{Al}_2)\text{O}_{22}(\text{OH})_2$  and  $\text{NaCa}_2(\text{Fe}^{2+}_4\text{Fe}^{3+})(\text{Si}_6\text{Al}_2)\text{O}_{22}(\text{OH})_2$ , respectively (Hawthorne *et al.*, 2012). Compositions related to these root names are described by pargasite  $\text{NaCa}_2(\text{Mg}_4\text{Al})\text{Si}_6\text{Al}_2\text{O}_{22}(\text{OH})_2$  (Oberti *et al.*, 1995; Tait *et al.*, 2001; Heaveysege *et al.*, 2015), the ferric member magnesio-hastingsite  $\text{NaCa}_2(\text{Mg}_4\text{Fe}^{3+})\text{Si}_6\text{Al}_2\text{O}_{22}(\text{OH})_2$  (Walitzi & Walter, 1981), chromio-pargasite  $\text{NaCa}_2(\text{Mg}_4\text{Cr}^{3+})\text{Si}_6$

$\text{Al}_2\text{O}_{22}(\text{OH})_2$  (Nishio-Hamane *et al.*, 2012; Cámara *et al.*, 2015), and vanadio-pargasite (Reznitsky *et al.*, 2017; this study). Although not yet approved by IMA-CNMNC, the crystal structure of a natural  $C2/m$  pargasite with dominant  $\text{Mn}^{3+}$  as trivalent cation at the  $M(1)$ – $M(3)$  sites, ideally  $\text{NaCa}_2(\text{Mg}_4\text{Mn}^{3+})\text{Si}_6\text{Al}_2\text{O}_{22}(\text{OH})_2$ , was reported (Hålenius & Bosi, 2012). The ionic radius of the octahedral  $\text{Me}^{3+}$  ion at the  $M(1,2,3)$  sites varies in the sequence  $r^{[6]\text{Al}} = 0.535 < r^{[6]\text{Cr}} = 0.615 < r^{[6]\text{V}} = 0.640 < r^{[6]\text{Mn}} = 0.645 = r^{[6]\text{Fe}} = 0.645$  Å (Shannon, 1976). Synthetic analogues of pargasite with different trivalent cations (Raudsepp *et al.*, 1987, 1991) were also structurally characterized paying special attention to order–disorder of trivalent cations at the octahedral sites. In this study we report the crystal structure of the new mineral vanadio-pargasite. Structural features are discussed and compared to those of amphiboles with analogous composition.

## 2. Experimental methods

### 2.1. Infrared spectroscopy

A single-crystal unpolarized FTIR (Fourier-transform infrared) spectrum was recorded at room temperature using a Bruker Hyperion 3000 IR microscope equipped

Table 1. Crystal data and refinement parameters for vanadio-pargasite

Crystal data (room T)	
<i>a</i> (Å)	9.8956(1)
<i>b</i> (Å)	17.9970(2)
<i>c</i> (Å)	5.2970(1)
$\beta$ (°)	105.391(1)
Cell volume (Å <sup>3</sup> )	909.52(2)
<i>Z</i>	2
Space group	<i>C2/m</i>
Refined formula	Na <sub>1.0</sub> Ca <sub>1.96</sub> (Mg <sub>4.31</sub> V <sup>3+</sup> <sub>0.68</sub> ) [Si <sub>6</sub> Al <sub>2</sub> O <sub>22</sub> ](OH <sub>1.67</sub> F <sub>0.33</sub> )
Chemical formula*	(K <sub>0.07</sub> Na <sub>0.90</sub> )(Na <sub>0.05</sub> Ca <sub>1.91</sub> Mg <sub>0.04</sub> ) $\Sigma$ 2.00 (Mg <sub>4.02</sub> Cr <sub>0.05</sub> V <sub>0.68</sub> Al <sub>0.23</sub> Ti <sub>0.02</sub> ) $\Sigma$ 5.00 (Si <sub>6.09</sub> Al <sub>1.91</sub> ) $\Sigma$ 8.00O <sub>22</sub> (OH <sub>1.67</sub> F <sub>0.33</sub> ) $\Sigma$ 2.00
Intensity measurement	
Diffractometer	APEX II SMART
X-ray radiation	MoK $\alpha$ $\lambda$ = 0.71073 Å
X-ray power	50 kV, 30 mA
Monochromator	Graphite
Temperature	25 °C
Time per frame	10 s
Max. $\theta$ °	48.0
Index ranges	$-18 \leq h \leq 19$ $-36 \leq k \leq 36$ $-11 \leq l \leq 8$
No. of measured reflections	14645
No. of unique reflections	4081
No. of observed reflections $I > 2\sigma(I)$	3920
Structure refinement	
No. of parameters refined	115
<i>R</i> (int)	0.0218
<i>R</i> ( $\sigma$ )	0.0195
GooF	1.31
<i>R</i> <sub>1</sub> , $I > 2\sigma(I)$	0.0181
<i>R</i> <sub>1</sub> , all data	0.0194
<i>wR</i> <sub>2</sub> (on <i>F</i> <sup>2</sup> )	0.0480
$\Delta\rho_{\min}$ ( $-e \cdot \text{Å}^{-3}$ ) close to	-0.44 <i>T</i> (2)
$\Delta\rho_{\max}$ ( $-e \cdot \text{Å}^{-3}$ ) close to	0.79 H

\* Reznitsky *et al.* (2017)

with a N<sub>2</sub>-cooled MCT detector at INFN (Frascati, Rome). The microscope was attached to a Bruker V70 optical bench; a Globar IR source and a KBr beamsplitter were used. The aperture was set to 100  $\mu\text{m}^2$  and 128 scans were averaged on both sample and background, with a nominal resolution of 4  $\text{cm}^{-1}$ .

## 2.2. Single-crystal X-ray diffraction

A single crystal of vanadio-pargasite (0.40  $\times$  0.15  $\times$  0.15 mm) of average chemical composition (K<sub>0.07</sub>Na<sub>0.90</sub>)(Na<sub>0.05</sub>Ca<sub>1.91</sub>Mg<sub>0.04</sub>) $\Sigma$ 2.00(Mg<sub>4.02</sub>Cr<sub>0.05</sub>V<sub>0.68</sub>Al<sub>0.23</sub>Ti<sub>0.02</sub>) $\Sigma$ 5.00(Si<sub>6.09</sub>Al<sub>1.91</sub>) $\Sigma$ 8.00O<sub>22</sub>(OH<sub>1.67</sub>F<sub>0.33</sub>) $\Sigma$ 2.00 (Reznitsky *et al.*, 2017) was glued on the tip of a glass fiber and mounted on a goniometer head. Diffraction data were collected using a Bruker SMART APEX II CCD diffractometer installed at the University of Bern. Intensity data were measured at room temperature using graphite-monochromatized MoK $\alpha$  radia-

tion ( $\lambda$  = 0.71069 Å). Preliminary lattice parameters and an orientation matrix were obtained from three sets of frames and refined during the integration process of the intensity data. Diffraction data were collected with  $\omega$  scans at different  $\phi$  settings ( $\phi$ - $\omega$  scan) (Bruker, 1999). Data were processed using SAINT (Bruker, 1999). An empirical absorption correction using SADABS (Sheldrick, 1996) was applied. The correct space group was *C2/m* in agreement with other amphiboles belonging to the compositional space of pargasite. The structure was solved by direct methods using SHELXTL 2008 (Sheldrick, 2008) and refinements were done using SHELXL 2013 (Sheldrick, 2015). Scattering factors for neutral atoms were used throughout. The coordinates corresponds to those used by Heaveysege *et al.* (2015) for pargasite. In order to determine the scattering power at the *A*, *M*(4), *M*(1), *M*(2), and *M*(3) sites, the following strategy based on the chemical composition was chosen. Direct occupancy refinement at *M*(1) and *M*(3) converged to full occupancy with Mg scattering factors, then the *M*(1) and *M*(3) occupancies were fixed at 1. The occupancy at *M*(2) was refined with Mg and V scattering factors. In doing so, Mg scattering factor was assumed to include also Al contribution, and that of V to include minor Cr contribution. Occupancy of the Ca scattering factors for the *M*(4) site were refined. Complete occupancy by Si was assigned to *T*(2) while 0.5 Si + 0.5 Al were applied to the occupancy of *T*(1). This in agreement with the double-chain composition (Si<sub>6</sub>Al<sub>2</sub>)O<sub>22</sub>. The electron density distribution around the *A* cavity was modelled by *A*(*m*) and *A*(2). Both *A* sites were refined with anisotropic displacement parameters. Minor K content determined by chemical analyses was not assigned and was assumed as modelled by the Na scattering factor. The H position close to O(3) was obtained from difference-Fourier maps and refined isotropically without restraints on O–H distance. The analyzed F content of 0.33 atom per formula unit (*apfu*) located at O(3) was taken into account by refining the O(3) site with 0.17 F + 0.83 O scattering factors. Data-collection parameters are reported in Table 1. A corresponding cif file is deposited as Supplementary Material, linked to this article and freely available at <https://pubs.geoscienceworld.org/eurjmin/>.

## 3. Results

### 3.1. Structure refinement

Atomic coordinates, occupancy and isotropic displacement parameters of vanadio-pargasite are reported in Table 2. Table 3 shows the anisotropic displacement parameters, and Table 4 selected interatomic distances; both tables are deposited and freely available as part of the Supplementary Material. Bond-valence analysis is reported in Table 5. Vanadio-pargasite is monoclinic *C2/m* (Fig. 1), with unit-cell parameters *a* = 9.8956(1), *b* = 17.9970(2), *c* = 5.2970(1) Å,  $\beta$  = 105.391(1)°, and *V* = 909.52 Å<sup>3</sup>.

Our refinement allowed to determine the H position of the hydroxyl group at O(3) (Table 2). The oxygen at O(7) acts as an acceptor for the hydrogen bond, with

Table 2. Atom coordinates, equivalent displacement parameters  $U^{eq}$  ( $\text{\AA}^2$ ), and refined occupancies of vanadio-pargasite.

Site	Atom	<i>x</i>	<i>y</i>	<i>z</i>	$U^{eq}$	Occ.
<i>T</i> (1)	0.5 Si + 0.5 Al	0.28074(2)	0.08533(2)	0.30321(3)	0.00498(3)	1
<i>T</i> (2)	Si	0.29066(2)	0.17308(2)	0.81298(2)	0.00512(3)	1
<i>M</i> (1)	Mg	0	0.08891(2)	0.5	0.00569(4)	1
<i>M</i> (2)	0.344(2) V + 0.656(2) Mg	0	0.17545(2)	0	0.00468(5)	1
<i>M</i> (3)	Mg	0	0	0	0.00493(5)	1
<i>M</i> (4)	Ca	0	0.28005(2)	0.5	0.00808(3)	0.9717(12)
<i>A</i> (2)	Na	0	0.4685(3)	0	0.0260(11)	0.201(8)
<i>A</i> ( <i>m</i> )	Na	0.0241(7)	0.5	0.0520(12)	0.054(2)	0.306(8)
O(1)	O	0.10676(4)	0.08756(2)	0.21731(7)	0.00758(5)	1
O(2)	O	0.12021(4)	0.17312(2)	0.73108(7)	0.00692(5)	1
O(3)	0.83 O + 0.17 F	0.10751(5)	0	0.71598(10)	0.00825(7)	1
O(4)	O	0.36658(4)	0.25026(2)	0.78806(7)	0.00884(5)	1
O(5)	O	0.35021(4)	0.14093(2)	0.11286(7)	0.01040(6)	1
O(6)	O	0.34493(4)	0.11629(2)	0.61275(8)	0.01103(6)	1
O(7)	O	0.34179(6)	0	0.27502(12)	0.01288(8)	1
H	H	0.199(3)	0	0.767(5)	0.031(6)	0.832

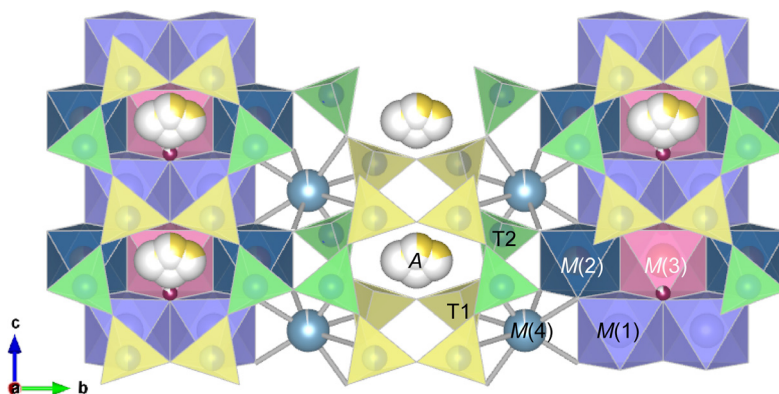


Fig. 1. Crystal structure of vanadio-pargasite,  $\text{NaCa}_2(\text{Mg}_4\text{V}^{3+})\text{Si}_6\text{Al}_2\text{O}_{22}(\text{OH})_2$ , projected along the *a* axis (VESTA: Momma & Izumi, 2011). *M*(2) is occupied by  $\text{V}^{3+}$  and other trivalent cations whereas *M*(1) and *M*(3) are mainly occupied by Mg; *M*(4) is occupied by Ca. *T*(1) is almost 1:1 occupied by Si and Al whereas *T*(2) site is occupied only by Si. The Na distribution around the *A* site was modelled by the split positions *A*(*m*) and *A*(2). The H site is shown as a purple sphere.

Table 5. Bond-valence analysis (*v.u.*) (following Brese & O'Keeffe, 1991) of vanadio-pargasite weighted on the refined occupancies. The contribution of the O–H bond has been evaluated according to Ferraris & Ivaldi (1988). The minor F substitution at O(3) is not considered.

	<i>T</i> (1)	<i>T</i> (2)	<i>M</i> (1)	<i>M</i> (2)	<i>M</i> (3)	<i>M</i> (4)	<i>A</i> (2)	<i>A</i> ( <i>m</i> )	H	$\Sigma$	$\Sigma(\text{H})$
O(1)	0.941		0.382 $\times 2 \downarrow$	0.376 $\times 2 \downarrow$	0.363 $\times 4 \downarrow$					2.06	
O(2)		0.994	0.327 $\times 2 \downarrow$	0.364 $\times 2 \downarrow$		0.296 $\times 2 \downarrow$				1.98	
O(3)			0.345 $\times 2 \downarrow \rightarrow$		0.371 $\times 2 \downarrow$				0.8	1.06	1.86
O(4)		1.064		0.457 $\times 2 \downarrow$		0.373 $\times 2 \downarrow$				1.89	
O(5)	0.867	0.943				0.176 $\times 2 \downarrow$	0.043 $\times 2 \downarrow$	0.020 $\times 2 \downarrow$		2.05	
O(6)	0.873	0.904				0.189 $\times 2 \downarrow$	0.036 $\times 2 \downarrow$	0.037 $\times 2 \downarrow$		2.04	
O(7)	0.913 $\times 2 \rightarrow$						0.066 $\times 2 \downarrow$	0.117+0.105 $\downarrow$	0.2	2.00	2.20
$\Sigma$	3.59	3.90	2.11	2.39	2.19	2.07	0.29	0.34	1		

corresponding  $\text{H}\cdots\text{A}$  and  $\text{D}\cdots\text{A}$  distances of 2.69(3) and 3.2403(8) Å, respectively. Such long distances and the DHA angle of  $122(2)^\circ$  indicate the weak nature of the hydrogen bond.

Vanadio-pargasite contains significant amounts of [4]-coordinated Al (Table 1). The observed  $\langle T(1)\text{--O} \rangle = 1.6776$  Å and  $\langle T(2)\text{--O} \rangle = 1.6337$  Å bond distances (Table 4) indicate that Al is strongly ordered at the *T*(1) site, in agreement with

Table 6. Refined site scattering (*epfu*) and site population (*apfu*) for vanadio-pargasite.

Site	Refined site population	Refined site scattering (SC-XRD)	Assigned site population	Calculated site-scattering
<i>M</i> (1)	Mg	24	2 Mg	24
<i>M</i> (2)	0.34V + 0.66Mg	15.6 + 15.8 = 31.4	1 Mg + 0.7 V + 0.3 Al	12 + 16.1 + 3.9 = 32
<i>M</i> (3)	Mg	12	1 Mg	12
		$\sum$ 67.4		$\sum$ 68
<i>M</i> (4)	Ca	38.8	1.91 Ca + 0.05 Na + 0.04 Mg	38.2 + 0.5 + 0.5 = 39.4
<i>A</i> (2)	Na	4.4	0.4 Na	4.4
<i>A</i> ( <i>m</i> )	Na	6.6	0.1 K + 0.5 Na	1.9 + 5.5 = 7.4
		$\sum$ <i>A</i> 11.0		$\sum$ <i>A</i> 11.8

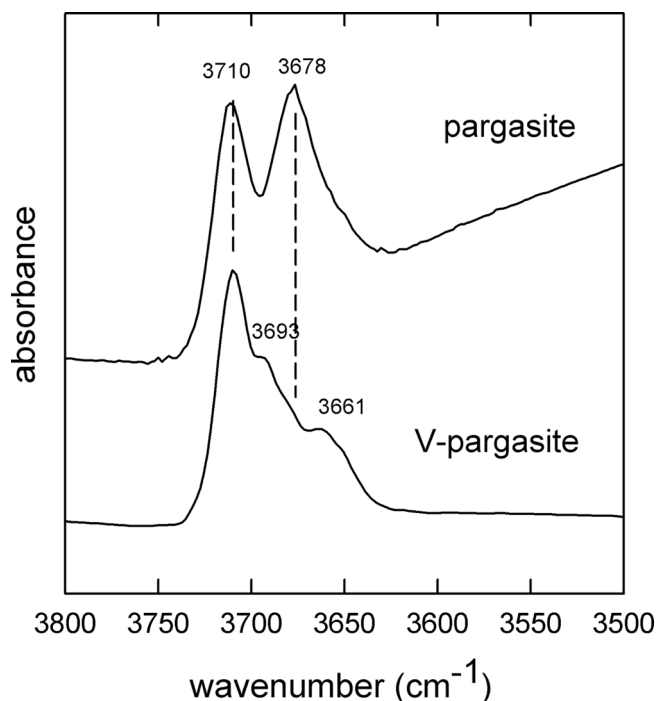


Fig. 2. The OH-stretching FTIR spectrum of vanadio-pargasite (this work) compared with the spectrum of synthetic end-member pargasite (data from Della Ventura *et al.*, 1999).

previous studies (*e.g.* Hawthorne & Oberti, 2007). The observed value  $\langle\langle T-O \rangle\rangle = 1.650 \text{ \AA}$  (*i.e.*  $(\langle T(1)-O \rangle + \langle T(2)-O \rangle)/2$ ) agrees with the theoretical one  $\langle\langle T-O \rangle\rangle = 1.654 \text{ \AA}$ , estimated by the equation proposed by Hawthorne & Oberti (2007):  $\langle\langle T-O \rangle\rangle = 1.6250 + 0.0153^{[4]}Al$ .

The distribution of the C-group cations at the octahedral sites *M*(1), *M*(2) and *M*(3) is reported in Table 6. The total refined scattering (67.4 *epfu*) is in good agreement with that (68 *epfu*) calculated from electron microprobe data. Our structural refinement indicates complete order of  $V^{3+}$  at the *M*(2) site, in agreement with the observed ordering of trivalent transition metal cations at the *M*(2) site in the majority of clino-amphiboles (Ghose *et al.*, 1986; Oberti & Ghose, 1993). The  $\langle M-O \rangle$  bond distances (Table 4) are 2.080, 2.053 and 2.066 Å for *M*(1), *M*(2), and *M*(3), respectively, confirming that the  $V^{3+}$  cation ( $r = 0.64 \text{ \AA}$ ; Shannon, 1976) occupies the *M*(2) octahedron.

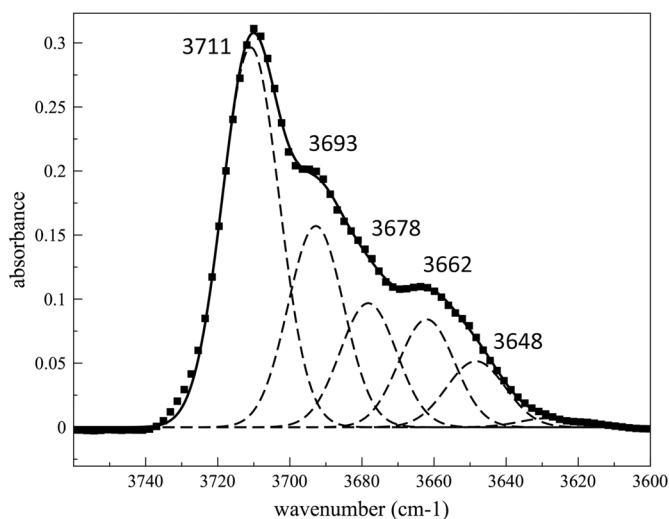


Fig. 3. The OH-stretching FTIR spectrum of vanadio-pargasite resolved into Gaussian components (broken lines). Squares, experimental data; full line, sum of fitted components.

The *M*(4) site showed slightly lower occupancy ( $19.4 e^-$ ) than expected ( $20 e^-$ ) for Ca. Thus, the assumed low Na content at *M*(4) according to chemical composition ( $Na_{0.05}Ca_{1.91}Mg_{0.04}$ ) is verified (Table 6).

The A cations were distributed among the *A*(2) and *A*(*m*) positions, 0.648(4) Å apart. The total refined scattering of the A sites (*A*(2) + *A*(*m*)) = 11 *epfu*, agrees with the value calculated from the chemical formula ( $0.1K + 0.9Na = 11.8 \text{ epfu}$ ).

#### 4. OH-stretching FTIR spectroscopy

The OH-stretching ( $4000\text{--}3000 \text{ cm}^{-1}$ ) FTIR spectrum of the studied amphibole is compared in Fig. 2 with that of synthetic end-member pargasite from Della Ventura *et al.* (1999). Three peaks can be clearly identified in the spectrum of vanadio-pargasite, centered at  $\sim 3710$ , 3693, and  $3661 \text{ cm}^{-1}$ , respectively; evident shoulders at  $\sim 3680$  and  $3650 \text{ cm}^{-1}$  indicate that additional components are likely to be hidden under the spectral envelope. The pattern was resolved by fitting Gaussian bands (Della Ventura, 2017) and the result is given in Fig. 3. Setting as unique constraint the FWHMs (full width at half

maximum height) to be roughly equal for all components at values reasonable for these compounds (Della Ventura *et al.*, 1999), five bands can be recognized in the pattern, centered at 3711, 3693, 3678, 3662 and 3648  $\text{cm}^{-1}$ , respectively (Fig. 3).

The interpretation of the FTIR spectrum of the studied amphibole is based on the relatively large amount of available data on synthetic pargasites with different compositions (*e.g.* Raudsepp *et al.*, 1987; Della Ventura *et al.*, 1999; Fialips-Guédon *et al.*, 2000; Hawthorne & Della Ventura, 2007).

The OH-stretching pattern of end-member pargasite (Fig. 2) displays two bands at 3710 and 3678  $\text{cm}^{-1}$  (Raudsepp *et al.*, 1987; Della Ventura *et al.*, 1999; Fialips-Guédon *et al.*, 2000); these are associated with O–H groups directly bonded with  $M^{(1)}\text{Mg}^{M(1)}\text{Mg}^{M(3)}\text{Mg}$  and  $M^{(1)}\text{Mg}^{M(1)}\text{Mg}^{M(3)}\text{Al}$  octahedral trimers, respectively, close to  $T^{(1)}\text{Si}-\text{O}(7)-T^{(1)}\text{Al}$  bridges and facing an alkali cation at the *A*-site (Della Ventura *et al.*, 1999, 2003, 2014); these configurations are indicated as  $M^{(1)}\text{Mg}^{M(1)}\text{Mg}^{M(3)}\text{Mg}-\text{SiAl}-\text{A}$  and  $M^{(1)}\text{Mg}^{M(1)}\text{Mg}^{M(3)}\text{Al}-\text{SiAl}-\text{A}$  in spectroscopic notation (Della Ventura *et al.*, 1999). In synthetic pargasite the *M*(3) occupancy is 0.5 Mg + 0.5 Al, thus the two bands have equal intensity (Fig. 3). In vanadio-pargasite the  $M^{(1)}\text{Mg}^{M(1)}\text{Mg}^{M(3)}\text{Mg}-\text{SiAl}-\text{A}$  band is the most intense in the spectrum in accordance with the X-ray data given above that indicate complete order of V at *M*(2). The band at 3678  $\text{cm}^{-1}$ , due to  $M^{(1)}\text{Mg}^{M(1)}\text{Mg}^{M(3)}\text{Al}-\text{SiAl}-\text{A}$  configurations, has a relatively lower intensity (Fig. 3); its presence in the spectrum, however, indicates that minor but significant Al occurs at *M*(3). Figure 3 shows that both bands are indeed associated with a second component shifted  $\sim 20 \text{ cm}^{-1}$  toward lower frequency, at 3693 and 3662  $\text{cm}^{-1}$ , respectively. This splitting can be assigned either to a next-nearest-neighbor (NNN) effect due to trivalent cations at *M*(2) or to local OH–F arrangements (Robert *et al.*, 2000; Heaveysege *et al.*, 2015). In the first case a shift of the O–H band of  $\sim 10 \text{ cm}^{-1}$  is observed (*e.g.* Della Ventura *et al.*, 1999), while in the second case the shift is  $\sim 20 \text{ cm}^{-1}$  (Robert *et al.*, 2000). On this basis, and considering the chemical composition of the studied sample, we assign the 3693 and 3662  $\text{cm}^{-1}$  bands to the  $M^{(1)}\text{Mg}^{M(1)}\text{Mg}^{M(3)}\text{Mg}-\text{SiAl}-\text{A}-\text{OH}-\text{F}$  and  $M^{(1)}\text{Mg}^{M(1)}\text{Mg}^{M(3)}\text{Al}-\text{SiAl}-\text{A}-\text{OH}-\text{F}$  configurations, respectively. Note that the measured frequencies of the 3711–3693 and 3678–3662  $\text{cm}^{-1}$  pair of components are exactly coincident with those measured by Robert *et al.* (2000) for F–OH substituted synthetic pargasites. The band at 3648  $\text{cm}^{-1}$ , finally, can be assigned to the presence of minor *A*-site vacancy (around 0.03 *apfu* from the relative band area, corrected for the 2.2 coefficient due to the difference in the absorption coefficient between the two bands, see Hawthorne *et al.*, 1997) in the structure (Fialips-Guédon *et al.*, 2000), in close agreement with the proposed crystal-chemical formula.

Table 7. Theoretical  $\langle M-\text{O} \rangle$  distances of vanadio-pargasite obtained from the site populations based on the  $\langle \text{cation}-\text{O} \rangle$  distances optimized for [6]-coordination and corrected for F effect at O(3) (Mg–O = 2.078 Å, V–O = 2.0255 Å, and Al–O = 1.929 Å, Oberti *et al.*, 2007).

	$\langle M-\text{O} \rangle$ calculated	$\langle M-\text{O} \rangle$ SC-XRD
$\langle M(1)-\text{O} \rangle$	2.076	2.081(2)
$\langle M(2)-\text{O} \rangle$	2.037	2.052(2)
$\langle M(3)-\text{O} \rangle$	2.076	2.066(3)

## 5. Discussion

In the recent years, there has been extensive research on  $^{[6]}\text{Me}^{3+}$  order–disorder over the *M*(1), *M*(2) and *M*(3) sites in pargasite. Although studies done on synthetic amphiboles (Raudsepp *et al.*, 1987, 1991) demonstrated that  $\text{Me}^{3+}$  cations ( $\text{Me}^{3+} = \text{Cr}, \text{Sc}, \text{Ga}, \text{In}$ ) are disordered over the three octahedral sites in hydroxyl (O(3)=OH) pargasite, more recent studies show that high-charge cations are ordered at *M*(2) in the absence of the oxo component. Partial disorder of  $^{[6]}\text{Al}$  over *M*(2) and *M*(3) was reported for both synthetic (Welch *et al.*, 1994; Della Ventura *et al.*, 1999) and natural Mg-rich pargasite (Oberti *et al.*, 1995; Tait *et al.*, 2001; Heaveysege *et al.*, 2015). Fialips-Guédon *et al.* (2000) synthesized (900 °C and 3 kbar) pargasitic amphiboles along the Al–Cr $^{3+}$  substitutional join and assumed, on the basis of the FTIR patterns, the preference of Cr $^{3+}$  for the *M*(3) site. This assignment is in contrast with the data of Oberti *et al.* (1995) and Nishio-Hamane *et al.* (2012) showing complete order of Cr $^{3+}$  at *M*(2) in chromium-rich pargasitic amphiboles.

Our results show that V $^{3+}$  is ordered at *M*(2) in vanadio-pargasite. This assignment is based on the site-scattering refinement considering that Mg (12 electrons) and V (23 electrons) have significantly different scattering factors thus allowing confident site-occupancy refinements. Analysis of the FTIR spectrum also excludes the presence of V at the OH-coordinated *M*(1,3) octahedra. As reported above, occupancies of both *M*(1) and *M*(3) site converged to 1 using the scattering factors of Mg. Moreover, the  $\langle M(2)-\text{O} \rangle$  distance is the shortest (2.053 Å) among the  $\langle M(1,2,3)-\text{O} \rangle$  distances (Table 4). An ordered distribution of Cr $^{3+}$  at *M*(2) was also suggested for chromio-pargasite (Nishio-Hamane *et al.*, 2012) whereas in magnesio-hastingsite Fe $^{3+}$  was attributed to the *M*(3) site although the  $\langle M(2)-\text{O} \rangle = 2.047 \text{ Å}$  distance is significantly shorter compared to  $\langle M(3)-\text{O} \rangle = 2.073 \text{ Å}$ . Yet, the case of magnesio-hastingsite is more complex because this mineral also contains octahedral Fe $^{2+}$  replacing Mg. In the structure of “mangani-pargasite” (Hålenius & Bosi, 2012) the majority of Mn $^{3+}$  was also assigned to *M*(2) while additional Mn $^{3+}$  was assumed to occupy *M*(1) and *M*(3).

The theoretical  $\langle M-O \rangle$  distances (Table 7) were calculated from the site populations based on the  $\langle \text{cation}-O \rangle$  distances optimized for [6]-coordination and corrected for F effect at O(3) ( $\text{Mg}-O=2.078 \text{ \AA}$ ,  $\text{V}-O=2.0255 \text{ \AA}$ , and  $\text{Al}-O=1.929 \text{ \AA}$ , Oberti *et al.*, 2007). The obtained values of  $\langle M(1)-O \rangle=2.076$  (obs: 2.0808 Å) and  $\langle M(2)-O \rangle=2.037 \text{ \AA}$  (obs: 2.0529), are smaller than those obtained from structure refinement (Table 7), whereas the  $\langle M(3)-O \rangle=2.076$  distance is 0.010 Å longer than the observed one. Nevertheless, the calculated  $\langle M-O \rangle$  distances support that the  $M(2)$  octahedron is the one with the shortest  $\langle M-O \rangle$  distance and, as a consequence, the  $\text{Mn}^{3+}$  cation is expected to be ordered at this site. We also attributed 0.3 Al *pfu* to the  $M(2)$  site (Table 6) meaning that 15% Al ( $r^{[6]\text{Al}}=0.535 \text{ \AA}$ ) contributes to the mean ionic radius  $\langle r^{M(2)} \rangle$ . FTIR spectroscopy shows that minor  $^{[6]}\text{Al}$  is disordered at  $M(3)$ .

**Acknowledgements:** We would like to acknowledge the careful review of Roberta Oberti, which highly contributed to improve the manuscript.

## References

- Breese, N.E. & O’Keeffe, M. (1991): Bond-Valence parameters for solids. *Acta Crystallogr.*, **B47**, 192–197.
- Bruker (1999): SMART and SAINT-Plus. Versions 6.01. Bruker AXS Inc., Madison, Wisconsin, USA.
- Cámara, F., Gané, O.C., Belakovskiy, D.I., Uvarova, Y. (2015): New mineral names. *Am. Mineral.*, **100**, 1319–1332.
- Della Ventura, G. (2017): The analysis of asbestos minerals using vibrational spectroscopies (FTIR, Raman): crystal-chemistry, identification and environmental applications. in “Mineral fibres: crystal chemistry, chemical-physical properties, biological interactions and toxicity. EMU Notes in Mineralogy” A. Gualtieri ed., **18**, 135–169. DOI: [10.1180/EMU-notes.18.5](https://doi.org/10.1180/EMU-notes.18.5)
- Della Ventura, G., Hawthorne, F. C., Robert, J.L., Delbove, F., Welch, M.F., Raudsepp, M. (1999): Short-range order of cations in synthetic amphiboles along the richterite-pargasite join. *Eur. J. Mineral.*, **11**, 79–94.
- Della Ventura, G., Hawthorne, F.C., Robert, J.-L., Iezzi, G. (2003): Synthesis and infrared spectroscopy of amphiboles along the tremolite – pargasite join. *Eur. J. Mineral.*, **15**, 341–347.
- Della Ventura, G., Bellatreccia, F., Cámara, F., Oberti, R. (2014): Crystal-chemistry and short-range order of fluoro-edenite and fluoro-pargasite: a combined X-ray diffraction and FTIR spectroscopic approach. *Mineral. Mag.*, **78**, 293–310.
- Ferraris, G. & Ivaldi, G. (1988): Bond valence vs. bond length in O...O hydrogen bonds. *Acta Crystallogr.*, **B44**, 341–344.
- Fialips-Guédon, C. I., Robert, J.L., Delbove, F. (2000): Experimental study of Cr incorporation in pargasite. *Am. Mineral.*, **85**, 687–693.
- Ghose, S., Kersten, M., Langer, K., Rossi, G., Ungaretti, L. (1986): Crystal field spectra and Jahn Teller effect of  $\text{Mn}^{3+}$  in clinopyroxene and clin amphiboles from India. *Phys. Chem. Minerals*, **13**, 291–305.
- Hålenius, U. & Bosi, F. (2012): Cation ordering in  $\text{Pb}^{2+}$ -bearing,  $\text{Mn}^{3+}$ -rich pargasite from Långban, Sweden. *Am. Mineral.*, **97**, 1635–1640.
- Hawthorne, F.C. & Della Ventura, G. (2007): Short-range order in amphiboles. *Rev. Miner. Geochem.*, **67**, 173–222.
- Hawthorne, F. C. & Oberti, R. (2007): Amphiboles: Crystal Chemistry. *Rev. Miner. Geochem.*, **67**, 1–54.
- Hawthorne, F.C., Della Ventura, G., Robert, J.-L., Welch, M.D., Raudsepp, M., Jenkins, D.M. (1997): A Rietveld and infrared study of synthetic amphiboles along the potassium-richterite – tremolite join. *Am. Mineral.*, **82**, 708–716.
- Hawthorne, F. C., Oberti, R., Harlow, G. E., Maresch, W.V., Martin, R.F., Schumacher, J.C., Welch, M.D. (2012): Nomenclature of the amphibole supergroup. *Am. Mineral.*, **97**, 2031–2048.
- Heaveysege, D., Abdu, Y.A., Hawthorne, F.C. (2015): Long-range and short-range order in gem pargasite from Myanmar: crystal structure refinement and infrared spectroscopy. *Can. Mineral.*, **53**, 497–510.
- Momma, K. & Izumi, F. (2011): VESTA 3 for three-dimensional visualization of crystal, volumetric and morphology data. *J. Appl. Crystallogr.*, **44**, 1272–1276.
- Nishio-Hamane, D., Ohnishi, M., Minakawa, T., Yamaura, J., Saito, S., Kadota, R. (2012): Ehimeite,  $\text{NaCa}_2(\text{Mg}_4\text{Cr}^{3+})\text{Si}_6\text{Al}_2\text{O}_{22}(\text{OH})_2$ : the first Cr-dominant amphibole from the Akaishi Mine, Higashi-Akaishi Mountain, Ehime Prefecture, Japan. *J. Miner. Petrol. Sci.*, **107**, 1–7.
- Oberti, R. & Ghose, S. (1993): Crystal chemistry of a complex Mn bearing alkali amphibole (“tirodite”) on the verge of exsolution. *Eur. J. Mineral.*, **5**, 1153–1160.
- Oberti, R., Hawthorne, F.C., Ungaretti, L., Cannillo, E. (1995):  $^{[6]}\text{Al}$  disorder in amphiboles from mantle peridotites. *Can. Mineral.*, **33**, 867–878.
- Oberti, R., Hawthorne, F.C., Cannillo, E., Cámara, F. (2007): Long-range order in amphiboles. *Rev. Miner. Geochem.*, **67**, 125–171.
- Raudsepp, M., Turnock, A.C., Hawthorne, F.C., Sheriff, B., Hartman, J.S. (1987): Characterization of synthetic pargasitic amphiboles ( $\text{NaCa}_2\text{Mg}_4\text{M}^{3+}\text{Si}_6\text{Al}_2\text{O}_{22}(\text{OH}, \text{F})_2$ ;  $\text{M}^{3+} = \text{Al}, \text{Cr}, \text{Ga}, \text{Sc}, \text{In}$ ) by infrared spectroscopy, Rietveld structure refinement, and  $^{27}\text{Al}$ ,  $^{29}\text{Si}$  and  $^{19}\text{F}$  MAS NMR spectroscopy. *Am. Mineral.*, **72**, 580–593.
- Raudsepp, M., Turnock, A. C., Hawthorne, F. C. (1991): Amphibole synthesis at low pressure: what grows and what doesn’t. *Eur. J. Mineral.*, **3**, 983–1004.
- Robinson, K., Gibbs, G. V., Ribbe, P. H. (1971): Quadratic elongation: A quantitative measure of distortion in coordination polyhedra. *Science*, **172**, 567–570.
- Reznitsky, L.Z., Sklyarov E.V., Cametti G., Armbruster T., Suvorova L.F., Ushchapovskaya Z.F., Barash I.G. (2017): Vanadio-pargasite  $\text{NaCa}_2\text{Mg}_4\text{V}(\text{Si}_6\text{Al}_2)\text{O}_{22}(\text{OH})_2$  a new mineral of amphibole group. *Zapiski Russian Mineralogical Society*, **146**, 62–74.
- Robert, J.-L., Della Ventura, G., Welch, M., Hawthorne, F.C. (2000): OH-F substitution in synthetic pargasite at 1.5 kbar, 850 °C. *Am. Mineral.*, **5**, 926–931.

- Shannon, R.D. (1976): Revised effective ionic radii and systematic studies of interatomic distances in halides and chalcogenides. *Acta Crystallogr.*, **A32**, 751–767.
- Sheldrick, G.M. (1996): SADABS. University of Göttingen, Germany.
- (2008): A short history of SHELX. *Acta Crystallogr.*, **A64**, 112–122.
- (2015): Crystal structure refinement with *SHELX*. *Acta Crystallogr.*, **C71**, 3–8.
- Tait, K. T., Hawthorne, F.C., Della Ventura, G. (2001): Al-Mg disorder in a gem-quality pargasite from Baffin Island, Nunavut, Canada. *Can. Mineral.*, **39**, 1725–1732.
- Walitzi, E.M. & Walter, F. (1981): Verfeinerung der Kristallstruktur eines basaltischen Magnesio-Hastingsites. *Z. Kristallogr.*, **156**, 197–208.
- Welch, M.D., Kolodziejski, W., Klinowski, J. (1994): A multinuclear study of synthetic pargasite. *Am. Mineral.*, **79**, 261–268.

Received 19 September 2017

Modified version received 19 December 2017

Accepted 28 December 2017